

## Distinguishing Emission-Associated Ambient Air PM<sub>2.5</sub> Concentrations and Meteorological Factor-Induced Fluctuations

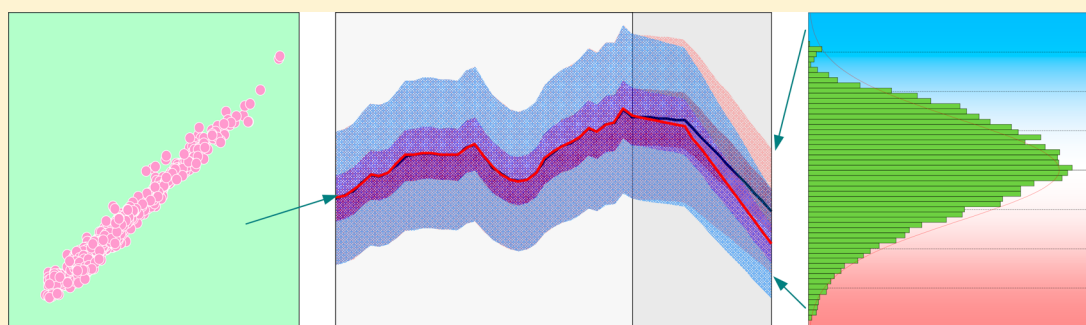
Qirui Zhong,<sup>†</sup> Jianmin Ma,<sup>†</sup> Guofeng Shen,<sup>†</sup> Huizhong Shen,<sup>†</sup> Xi Zhu,<sup>†</sup> Xiao Yun,<sup>†</sup> Wenjun Meng,<sup>†</sup> Hefa Cheng,<sup>†</sup> Junfeng Liu,<sup>†</sup> Bengang Li,<sup>†</sup> Xilong Wang,<sup>†</sup> Eddy Y. Zeng,<sup>Δ</sup> Dabo Guan,<sup>‡</sup> and Shu Tao<sup>\*,†</sup>

<sup>†</sup>College of Urban and Environmental Sciences, Laboratory for Earth Surface Processes, Sino-French Institute for Earth System Science, Peking University, Beijing 100871, China

<sup>Δ</sup>Guangdong Key Laboratory of Environmental Pollution and Health, School of Environment, Jinan University, Guangzhou 510632, China

<sup>‡</sup>School of International Development, University of East Anglia, Norwich, Norfolk NR4 7TJ, U.K.

### S Supporting Information



**ABSTRACT:** Although PM<sub>2.5</sub> (particulate matter with aerodynamic diameters less than 2.5 μm) in the air originates from emissions, its concentrations are often affected by confounding meteorological effects. Therefore, direct comparisons of PM<sub>2.5</sub> concentrations made across two periods, which are commonly used by environmental protection administrations to measure the effectiveness of mitigation efforts, can be misleading. Here, we developed a two-step method to distinguish the significance of emissions and meteorological factors and assess the effectiveness of emission mitigation efforts. We modeled ambient PM<sub>2.5</sub> concentrations from 1980 to 2014 based on three conditional scenarios: realistic conditions, fixed emissions, and fixed meteorology. The differences found between the model outputs were analyzed to quantify the relative contributions of emissions and meteorological factors. Emission-related gridded PM<sub>2.5</sub> concentrations excluding the meteorological effects were predicted using multivariate regression models, whereas meteorological confounding effects on PM<sub>2.5</sub> fluctuations were characterized by probabilistic functions. When the regression models and probabilistic functions were combined, fluctuations in the PM<sub>2.5</sub> concentrations induced by emissions and meteorological factors were quantified for all model grid cells and regions. The method was then applied to assess the historical and future trends of PM<sub>2.5</sub> concentrations and potential fluctuations on global, national, and city scales. The proposed method may thus be used to assess the effectiveness of mitigation actions.

### INTRODUCTION

PM<sub>2.5</sub> (particulate matter with aerodynamic diameters of less than 2.5 μm) is a major environmental and health concern.<sup>1,2</sup> PM<sub>2.5</sub> in the air originates from the direct emissions of primary aerosols and from the secondary formation of aerosols from various precursors,<sup>3</sup> and ambient PM<sub>2.5</sub> concentrations are shaped primarily by emission rates.<sup>4–6</sup> In addition to emissions, meteorological conditions are critical to the formation and transport of PM<sub>2.5</sub> through the air.<sup>7–9</sup> Interannual climate variability can also affect regional pollution levels.<sup>10</sup> Therefore, spatiotemporal variations in PM<sub>2.5</sub> concentrations in the atmosphere are mainly driven by the combined effects of emissions, chemical reactions, and meteorology.<sup>11</sup>

Although the impacts of emissions and meteorological confounding effects on PM<sub>2.5</sub> pollution have been studied extensively,<sup>12–14</sup> a lack of understanding of interactions between them has often led to confusion among the public and policymakers. For example, local governments often report on the effectiveness of their mitigation efforts from observed reductions in annual mean PM<sub>2.5</sub> concentrations ignoring considerable fluctuations in meteorological conditions occurring between years. Such a practice is misleading whenever

Received: May 19, 2018

Revised: August 15, 2018

Accepted: August 17, 2018

Published: August 17, 2018

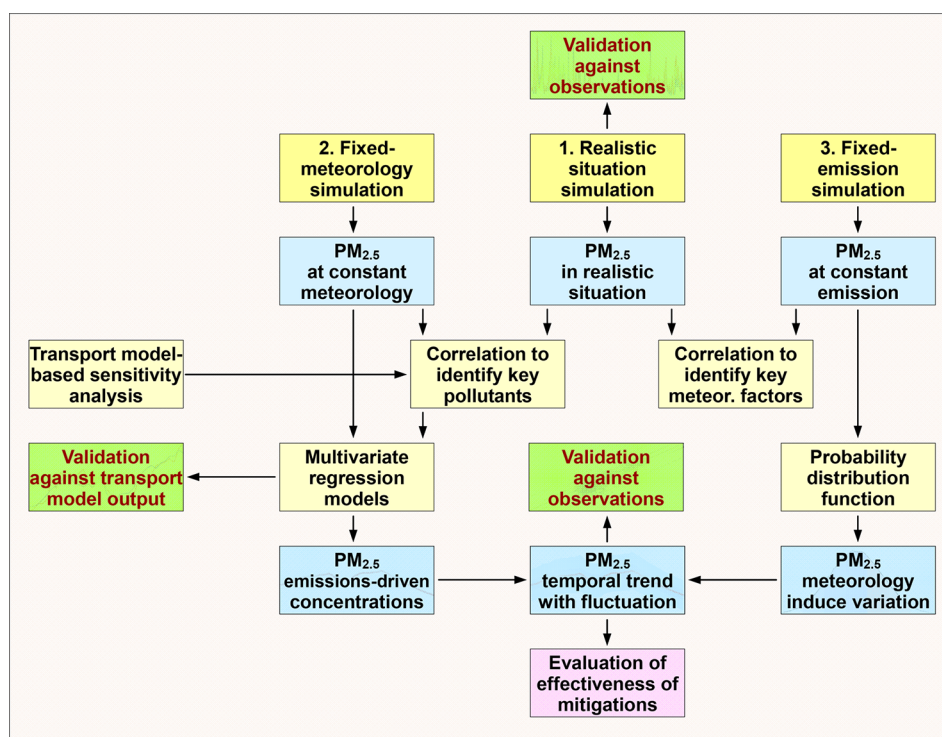


**Figure 1.** Flowchart showing the research scheme of this study. Gridded  $PM_{2.5}$  concentrations were simulated for the three scenarios from 1980 to 2014. Individual effects of emissions and meteorological factors were measured. Regression models were developed using the second model's scenario simulation output to predict gridded  $PM_{2.5}$  concentrations based on emissions. Meteorological confounding effect-induced variations were quantified as probabilistic functions using the third model's scenario simulation output. Using the models, trends in  $PM_{2.5}$  concentrations with a variability range were generated, and the effectiveness of mitigation measures were evaluated. The procedures were validated at various stages.

strong positive or negative meteorological interferences occur. For example, an abnormal increase in  $PM_{2.5}$  concentrations occurred following a period of  $PM_{2.5}$  decline in northern China in early 2017. The average  $PM_{2.5}$  concentration in the first half-year of 2017 ( $66 \mu\text{g}/\text{m}^3$ ) was slightly higher than that during the same period in 2016 ( $64 \mu\text{g}/\text{m}^3$ ) in Beijing although comprehensive mitigation efforts have been made in recent years. The event has stimulated debate on the effectiveness of recent mitigation actions<sup>15</sup> even though these efforts have already led to a continuous decrease in annual mean  $PM_{2.5}$  concentrations in this area in recent years.<sup>16</sup> A recent study has suggested that the abnormal increase during the first six months of 2017 was strongly associated with anomalies in humidity.<sup>17</sup>

To quantify the contributions of emissions and confounding meteorological factors to ambient  $PM_{2.5}$  concentrations, a two-step approach was developed. In brief, global  $PM_{2.5}$  concentrations from 1980 to 2014 were simulated based on three conditional modeling scenarios: (1) realistic conditions, (2) fixed meteorology (realistic daily emission estimates but fixed meteorological parameters for 2014), and (3) fixed emissions (realistic daily meteorological variables with mean emissions from 1980 to 2014). Based on the results of the simulations, regression models were developed for individual grid cells to predict emission-driven  $PM_{2.5}$  trends. Probabilistic functions were established to characterize superimposed meteorology-associated fluctuations. When the regression models and probabilistic function were combined,  $PM_{2.5}$  concentration trends induced by changes in emissions and meteorological factor-associated fluctuations could be distinguished. The effectiveness of emission mitigation measures

could thus be evaluated. Moreover, future trends of ambient  $PM_{2.5}$  concentrations can be predicted based on projected changes in emissions.

## METHODS

**Overall Approach.** Figure 1 shows the overall scheme of the proposed approach including (1) a simulation based on three scenarios and (2) the development of regression models and probabilistic functions.

**Atmospheric Chemical Transport Modeling and Validation.** The Model for Ozone and Related Chemical Tracers, version 4 (MOZART4) was applied to simulate daily  $PM_{2.5}$  concentrations from 1980 to 2014 on a global scale.<sup>18</sup> The model was set with a  $1.895^\circ$  (latitude)  $\times$   $1.875^\circ$  (longitude) horizontal resolution, with 28 vertical layers, and with a 15 min time step. The species considered include black carbon (BC), organic carbon (OC), unspecified  $PM_{2.5}$  (primary  $PM_{2.5}$  - BC - 1.3OC), secondary organic aerosol (SOA), sulfate, nitrate, ammonium, dust, and sea salt. Emissions were obtained from the Peking University (PKU) series for primary aerosols ( $PM_{2.5}$ , BC, and OC),  $SO_2$  (sulfur dioxide), and  $NO_x$  (nitrogen oxides).<sup>19</sup> Emissions drawn from other inventories were also used in this study, including  $NH_3$  and nonbiogenic nonmethane volatile organic carbon (NMVOC) data collected from Emissions Database for Global Atmospheric Research (EDGAR) and Hemispheric Transport of Air Pollution, version 2 (HTAPv2),<sup>20,21</sup> biogenic volatile organic carbon (VOC) data collected from MEGAN (Model of Emissions of Gases and Aerosols from Nature),<sup>22</sup> and open-field biomass burning emission data collected from GFED4.1 (Global Fire Emissions Database, version 4.1).<sup>23</sup> National

Centers for Environmental Prediction/National Centers for Atmospheric Research (NCEP/NCAR) reanalysis products<sup>24</sup> were used as offline meteorological inputs. Aerosol optical depths from Moderate Resolution Imaging Spectroradiometer (MODIS)<sup>25</sup> were used as a proxy to downscale the model-predicted parameters into a fine grid cell of  $0.125^\circ \times 0.125^\circ$ .<sup>26</sup> Model performance was evaluated against more than 220 000 daily monitoring data points collected from around the world (Figure S1), against time series observations for six major cities around the world (Figure S2), and against major components (Figure S3). It can be observed that the majority of data points fall around the 1:1 line without bias and that the deviation of the predicted concentrations from the observations increase as the time scale decreases. For the annual means primarily used in this study, 87% of data points are within the 2-fold range.

**Conditional Scenarios and Relative Contributions.** The simulation was conducted based on three conditional modeling scenarios. The control run was conducted using realistic emission estimates and meteorological fields. For the fixed-meteorological condition scenario, meteorological parameters for 2014 (a normal non-El Niño year) were applied to all years with realistic emission estimates data. For the fixed-emission scenario, 35-year-averaged emissions were applied to all years together with realistic meteorological conditions. Deviations in the fixed emissions and fixed meteorological condition simulations from the normal simulation (control run) were normalized to their respective fractions to quantify the overall contributions of emissions ( $RC_E$ ) and meteorological conditions ( $RC_M$ ) for a given region (from a grid cell to the globe) and for a given period (from a month to multiple years) of interest.

**Sensitivity Analysis.** A sensitivity analysis was conducted to identify major air pollutants governing ambient air  $PM_{2.5}$  concentrations through a preliminary simulation for January 2010 (monthly resolution). Modeling was repeatedly performed by reducing or enhancing the emissions of individual pollutants by 10%, 25%, 50%, 75%, or 100% each time. The 21 pollutants tested include primary  $PM_{2.5}$  (including primary BC, OC, and unspecified  $PM_{2.5}$ ),  $SO_2$ ,  $NH_3$ ,  $NO_x$ , CO,  $CH_3SCH_3$ ,  $C_6H_5(CH_3)$ , BIGALK (lumped alkanes with  $C > 3$ ),  $C_2H_4$ , BIGENE (lumped alkenes with  $C > 3$ ),  $C_3H_6$ ,  $CH_2O$ ,  $CH_3CHO$ ,  $CH_3OH$ ,  $CH_3COCH_2CH_3$ ,  $C_3H_8$ ,  $C_2H_5OH$ ,  $C_2H_6$ ,  $CH_3COCH_3$ ,  $C_{10}H_{16}$ , and  $C_5H_8$ . The results of the sensitivity analysis are listed in Table S1.

**Emission-Based Regression Model.** On the basis of the results of the sensitivity analysis, the four main air pollutants were used for regression model development. Using annual emissions of these pollutants as independent variables and  $PM_{2.5}$  concentrations from the fixed-meteorology simulation as a dependent variable for 35 years, multivariate regression models with both dependent and independent variables log-transformed were developed for individual grid cells to predict  $PM_{2.5}$  concentrations without meteorological confounding effects. The regression was established for all individual grid cells using data for 35 years. The uncertainty of the regression models based on the fixed-meteorology simulation was characterized by a 90% confidence interval of predicted  $PM_{2.5}$  concentrations. Model-predicted  $PM_{2.5}$  concentrations were compared against those calculated from the fixed-meteorology simulation (the same data set used for model development). The method cannot be applied to model  $PM_{2.5}$  variation on a relatively short time scale such as a daily scale, which can be affected by many occasional extreme emission or

meteorological events, as well as the nonlinearity of secondary formation of aerosol.

**Meteorology-Related Probabilistic Functions.** For each individual grid cell, the frequency distribution of the annual mean  $PM_{2.5}$  concentrations for a 35 year period derived from the fixed-emission simulation was used as a meteorology-related probabilistic function to quantify random variations of  $PM_{2.5}$  induced by changes in meteorology at each grid cell. The function can also be generated for a region (such as a country) at other time scales (such as a month) of interest. At 84% of all model grid cells, the probabilistic functions calculated follow a normal distribution with a zero mean ( $K-S$  test,  $p > 0.05$ ).

**Characterization of Emission-Driven Trends with Meteorology-Induced Fluctuations.** This was done by combining emission-based trends with meteorology-induced variations from 1980 to 2030. Using emissions and  $PM_{2.5}$  concentrations for 2014 as baselines, the grid cell-specific models were applied to project the trajectory of  $PM_{2.5}$  concentrations induced by given emission changes for all grid cells across the globe. When superimposed on predicted  $PM_{2.5}$  concentrations derived from regression models, variations induced by fluctuations in meteorological variables presented as  $UI_{50}$  (intervals between the 25th and 75th percentiles) and  $UI_{95}$  (intervals between the 2.5 and 97.5 percentiles) were derived using the distribution pattern discussed in the previous section. Prior to future projections, combined model simulations were conducted for a period from 1988 (when the first valid observation was available) to 2014 and were validated against 2940 field observations collected from Interagency Monitoring of Protected Visual Environments (IMPROVE) for the United States and from The European Monitoring and Evaluation Programme (EMEP) for European countries at an annual scale, and corresponding results are shown in Figure S4.

**Other Analysis.** Statistical analysis was conducted using SPSS 23.0<sup>27</sup> with a significance level of 0.05. Monte Carlo simulations were performed using MATLAB R2016b<sup>28</sup> to generate the frequency distribution functions associated with variation of meteorological parameters for individual grid cells.

**Limitations and Uncertainties.** The methodology is affected by limitations and uncertainties. For example, the emission inventories are subject to uncertainty, and meteorological conditions for a single year (2014) are not truly representative. Like other atmospheric chemical transport models,<sup>14</sup> MOZART cannot provide model uncertainty information, while Monte Carlo simulation for complex atmospheric chemistry modeling would be unrealistic because of the extremely high computation loading. Moreover, many physicochemical processes were not even included.<sup>29,30</sup> Contribution of SOA to  $PM_{2.5}$  formation is often underestimated by the modeling. To date, very limited multiple-year observation data are available on a global scale, which are critical for model validation. Last but not the least, the overall uncertainty of the two-step procedure was unable to be characterized because of the limitations listed above. Nevertheless, there is still room to further improve the method. In addition to updating the inventories, quantifications of the effects of individual pollutants and meteorological factors could help to mitigate such uncertainties.

## RESULTS AND DISCUSSION

**Effects of Emissions and Meteorological Factors.** On the basis of the results of a sensitivity analysis, the relative

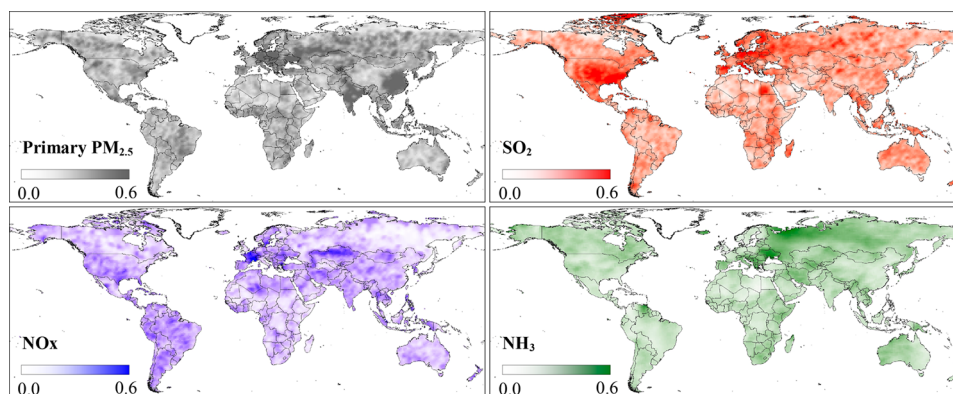


**Figure 2.** Geospatial distribution of partial correlation coefficients between the emissions of major air pollutants and  $\text{PM}_{2.5}$  concentrations. The four pollutants are primary  $\text{PM}_{2.5}$ ,  $\text{SO}_2$ ,  $\text{NO}_x$ , and  $\text{NH}_3$ .

contributions of various air pollutants to  $\text{PM}_{2.5}$  concentrations and the responses of  $\text{PM}_{2.5}$  to these pollutants are shown in Figure S5. As is shown, 97% of the variations in  $\text{PM}_{2.5}$  concentrations are attributable to the emission of primary  $\text{PM}_{2.5}$  ( $56.9 \pm 28.6\%$ ) followed by the emission of  $\text{SO}_2$  ( $18.9 \pm 8.8\%$ ),  $\text{NH}_3$  ( $12.9 \pm 6.6\%$ ), and  $\text{NO}_x$  ( $8.3 \pm 6.8\%$ ). Similar results have recently been reported.<sup>31,32</sup> Significant ( $p < 0.05$ ) correlations between the emissions of the four pollutants and  $\text{PM}_{2.5}$  concentrations derived from the fixed-meteorology simulation were found for 70% of land grid cells around the world, denoting the feasibility of predicting emission-driven  $\text{PM}_{2.5}$  concentrations based on emission densities of these pollutants while excluding confounding meteorological effects. Those land grid cells (30%) not showing significant correlations between pollutant emissions and ambient  $\text{PM}_{2.5}$  concentrations were mostly identified in desert areas and high-latitude regions with low emissions, such as the Sahara Desert and the Arctic Archipelago.

Figure 2 presents maps of partial correlation coefficients between emissions and  $\text{PM}_{2.5}$  concentrations on an annual basis. The four major pollutants in terms of their respective contribution to  $\text{PM}_{2.5}$  concentrations, including primary  $\text{PM}_{2.5}$ ,  $\text{SO}_2$ ,  $\text{NO}_x$ , and  $\text{NH}_3$ , are shown. Primary  $\text{PM}_{2.5}$ -dominated partial correlations were found for China and India, where coal and biomass fuels used for power generation, industry, residential sectors, and cement production are the most important emission sources.<sup>33,34</sup> In the United States,  $\text{PM}_{2.5}$  concentrations are more  $\text{SO}_2$  emission-dependent, which is consistent with the large fraction of sulfates in total  $\text{PM}_{2.5}$  concentrations observed in the country.<sup>35</sup> For most Western European countries, primary  $\text{PM}_{2.5}$  and  $\text{SO}_2$  made a synthetic contribution to  $\text{PM}_{2.5}$  mass concentration (such was the case in Germany<sup>36</sup>), whereas  $\text{NO}_x$  has a stronger effect on France. The influence of  $\text{NH}_3$  mainly occurred in Eastern European countries and Russia (west) because  $\text{NH}_3$  exhausted from the agriculture sector (e.g., fertilizer and domesticated animals) is the leading factor affecting formation of ammonium sulfate and nitrate.<sup>1</sup> The significance of the correlation increased as the time scale changed from annual to daily. For example, median correlation  $p$  values of  $\text{SO}_2$  are 0.14 (0.012–0.46), 0.011 (0.0000038–0.29), and  $9.4 \times 10^{-31}$  ( $3.1 \times 10^{-105}$ – $7 \times 10^{-7}$ ) on annual, monthly, and daily scales, respectively.

Similarly, significant partial correlations ( $p < 0.05$ ) were found between the main meteorological parameters and  $\text{PM}_{2.5}$  concentrations derived from the fixed-emission scenario simulation. On average, the most important parameter is air

temperature ( $T$ ), with a correlation of 0.22 followed by wind speed ( $WS$ ,  $r = -0.16$ ), planetary boundary layer height (PBLH,  $r = -0.16$ ), relative humidity ( $RH$ ,  $r = 0.14$ ), and surface pressure ( $SP$ ,  $r = -0.14$ ). These results correspond with those of a previous study.<sup>7,14,37</sup> The geospatial distribution of the main meteorological parameters is shown in Figure S6. In cold, high-latitude regions of North America and Siberia and in warm regions extending from northern Africa to the Arabian Peninsula,  $\text{PM}_{2.5}$  concentrations are mostly sensitive to temperature, which is partially associated with temperature-sensitive  $\text{SO}_2$ .<sup>38</sup> The effects of  $WS$  or PBLH are stronger in regions with relatively high elevations, where strong winds facilitate dispersion,<sup>7,14,37</sup> whereas the presence of low PBLH levels predict a stable atmosphere.<sup>39</sup>  $WS$  and PBLH are also important in many other regions, including Southeast Asia, Brazil, and the eastern seaboard of Australia, where tropical or subtropical monsoons prevail.<sup>40</sup> In dry inland regions such as central Eurasia, the formation of secondary  $\text{PM}_{2.5}$  is more sensitive to  $RH$ .<sup>41</sup> To characterize the relationship between emissions and meteorological effects, the relative contributions of emissions ( $\text{RC}_E$ ) and meteorological conditions ( $\text{RC}_M$ ) were measured across all model grid cells based on the results of the three conditional scenario simulations. The mean daily/weekly  $\text{RC}_M$  values for  $\text{PM}_{2.5}$  ( $68\% \pm 5\%/63\% \pm 5\%$ ) are much higher than the mean daily/weekly  $\text{RC}_E$  values for  $\text{PM}_{2.5}$  ( $32\% \pm 5\%/37\% \pm 5\%$ ) ( $p < 0.05$ ). Emissions become more significant on a seasonal/annual basis. For example, mean seasonal  $\text{RC}_E$  is  $54\% \pm 7\%$ . Changes in emissions on these longer time scales are largely driven by seasonal emission cycles<sup>23,42</sup> and by long-term socioeconomic patterns.<sup>43</sup>

In addition to annual mean  $\text{PM}_{2.5}$  concentrations, the number of severely polluted days (NSPD, defined as the number of days with daily  $\text{PM}_{2.5}$  values of  $>150 \mu\text{g}/\text{m}^3$ ) is of particular interest not only because the annual mean concentrations are significantly associated with these high values<sup>44</sup> but also because public responses to extreme conditions are stronger.<sup>45</sup> The occurrence of heavy pollution episodes is often associated with stable meteorological conditions, as emissions do not usually change dramatically on a daily basis.<sup>46</sup> Figure S7a compares temporal variations of the NSPD for Beijing (from the realistic-case simulation) to emissions of major air pollutants for the surrounding area (Beijing–Tianjin–Hebei) for the winter months from 2000 to 2014. Although the NSPD and emissions undergo similar increasing trends, they are not always synchronous on an

annual basis because of the influence of meteorological conditions. For example, a sharp increase in the NSPD observed from 2012 to 2013 was not driven by emission increases but by unusual meteorological conditions.<sup>46,47</sup> During that winter, the seasonal averaged WS dropped from a long-term mean of 2.94 to 2.33 m/s, and the number of days of abnormally high humidity (RH > 75%) and extremely low PBLH (<150 m) increased from 3% to 10% and from 6.3% to 8.4%, respectively (Figure S7b–f), favoring the growth of secondary aerosols and the accumulation of air pollutants at the ground level.<sup>48,49</sup>

**Emission-Based Prediction.** As discussed above, annual mean  $PM_{2.5}$  concentrations for the 35 year period derived from the fixed-meteorology simulation are significantly correlated with emissions observed across individual model grid cells. Such a correlation suggests that a set of regression models can be developed to predict  $PM_{2.5}$  concentrations based on emissions with meteorological confounding effects excluded. If such models can be validated against the output of the fixed-meteorology simulation, they can be applied to simulate historical  $PM_{2.5}$  trends based exclusively on emissions and to predict emission-driven future  $PM_{2.5}$  trends. As confounding meteorological effects are eliminated by these models, the proposed method enables us to evaluate the effectiveness of emission-reduction efforts. To do so, the emissions of the four most important air pollutants identified based on a sensitivity analysis, primary  $PM_{2.5}$ ,  $SO_2$ ,  $NH_3$ , and  $NO_x$  were used as independent variables in developing multivariate regression models, whereas  $PM_{2.5}$  concentrations derived from the fixed-meteorology simulation were used as a dependent variable. As both emission densities and  $PM_{2.5}$  concentrations are log-normally distributed (Figure S8), the multivariate regression models were fitted to all model grid cells using log-transformed data and were applied to calculate annual mean  $PM_{2.5}$  concentrations for these grid cells. As the formation of secondary aerosols in the air does not linearly respond to precursor emissions,<sup>3</sup> several nonlinear equations were tested with no significant improvements observed in the results. Given that the statistical regression models were established to predict annual  $PM_{2.5}$ , the nonlinearity of the secondary aerosol formation, which occurred in a short time ranging from seconds to diurnal, was filtered out by the annual means. As such, the following linear model was adopted:

$$\log PM_{2.5} = \sum a_i \log E_i + b$$

where  $PM_{2.5}$  is annual mean  $PM_{2.5}$  concentration;  $E_i$  are annual emissions of the  $i$ th pollutants;  $a_i$  and  $b$  are regression coefficients. Figure S9 shows the spatial distribution of  $R^2$  values of the regression models, indicating that results for areas characterized by high emission levels and population densities are much better ( $R^2$  values are close to 1) than those found for other regions, which is helpful in reducing overall uncertainty. The regression models were validated by plotting the predicted  $PM_{2.5}$  concentrations against those derived from the fixed-meteorology scenario simulation shown in Figure S10 for China, India, the United States, and Germany. This good agreement suggests that the models could be used to predict annual  $PM_{2.5}$  concentrations with reasonable accuracy, while confounding meteorological effects were not taken into account. It should be pointed out that the potential impact of climate change was not taken into consideration.

The simplified approach to predicting annual mean ambient  $PM_{2.5}$  concentrations at the ground level based on annual total emissions omits the exchanges occurring among grid cells due to transport. Although the association between the emissions and  $PM_{2.5}$  concentrations at a given grid cell can be disturbed by the atmospheric transport across grid cells, the influence of the atmospheric transport on the association is weakened by similarities among adjacent model grid cells. Such similarities were demonstrated by the spatial autocorrelation of the regression model parameters. On a global scale, the calculated Moran's autocorrelation indexes are valued at 0.39 (intercepts), 0.50 (slopes for primary  $PM_{2.5}$ ), 0.33 (slopes for  $SO_2$ ), 0.36 (slopes for  $NO_x$ ), and 0.30 (slopes for  $NH_3$ ) and are statistically significant ( $p < 0.05$ ). As was expected, such autocorrelation is also significant for the gridded emissions and  $PM_{2.5}$  concentrations, and Moran's autocorrelation indexes vary from 0.25 to 0.52 for gridded emissions of the four pollutants and are as high as 0.75 for gridded  $PM_{2.5}$  concentrations ( $p < 0.05$ ). The most significant autocorrelation of  $PM_{2.5}$  concentrations is attributed to the dispersion of  $PM_{2.5}$  in the air. Because of the autocorrelation of emissions, emissions observed at individual grid cells also shape emissions from the surrounding grid cells.

**Meteorology-Related Variations.** As discussed above, interannual trends of emission-driven  $PM_{2.5}$  concentrations excluding meteorological confounding effects can be predicted based on annual emissions from data generated from the fixed-meteorology simulation. Similarly, the outputs of the fixed-emission simulation provide the information on variations in  $PM_{2.5}$  concentrations caused by confounding meteorological effects. As the influence of meteorological factors randomly fluctuates based on emission-induced  $PM_{2.5}$  concentrations, the following probabilistic function was used to characterize such random effects:

$$F(PM_{2.5}) = (2\pi\sigma)^{-0.5} \exp(-PM_{2.5}^2/2\sigma^2)$$

where  $F(PM_{2.5})$  is a probability function,  $PM_{2.5}$  is the annual mean  $PM_{2.5}$  concentration, and  $\sigma$  is the standard deviation associated with change in meteorological conditions under the fixed emission. On the basis of annual mean  $PM_{2.5}$  concentrations calculated from the fixed-emission simulation for the 35 years spanning from 1980 to 2014, probabilistic functions were derived for all individual grid cells on an annual scale. For most of the grid cells (84%), the functions are normally distributed ( $p > 0.05$ ). Deviations from the normal distribution are mostly observed in deserts or surrounding areas (Figure S11). For the fixed-meteorology simulation, the year 2014 is assumed to be a "normal" year for which most meteorological parameters are approximately equal to the 35 year mean with a standardized deviation of  $0.12 \pm 0.25$ . This assumption is confirmed by calculating the average deviation of annual  $PM_{2.5}$  concentrations derived from 2014 meteorology trends to average values for 1980 to 2014 based on the fixed-emission simulation. It was found that relative deviations for 95% of all model grid cells are less than 5%, and the overall mean value of deviation for all grid cells is  $0.072\% \pm 1.1\%$  (mean and standard deviation), which is not significantly different from zero ( $p > 0.05$ ), as was expected. Therefore, the frequency distribution generated from the fixed-emission simulation represents random variations resulting from confounding meteorological effects. The robustness of the function was also tested using a Jackknife test for a randomly selected grid cell. The test was conducted 35 times by

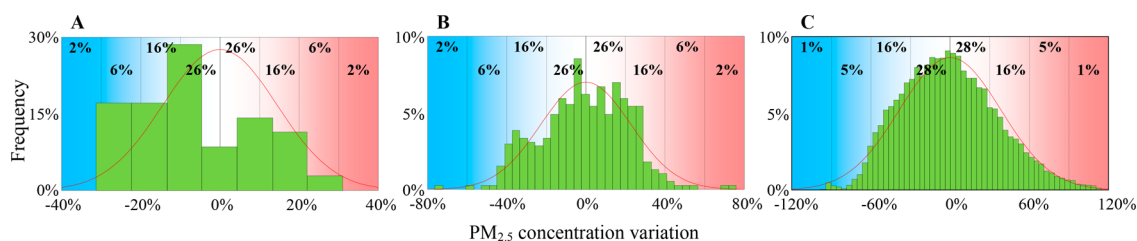


**Figure 3.** Probabilistic functions derived from fixed-emission simulations of annual (A), monthly (B), and daily resolutions (C) for a representative grid cell. Bars denote the frequency distribution of the model-calculated  $PM_{2.5}$  concentrations normalized by corresponding mean values with a fitted normal distribution curve. The probabilities of individual segments are shown in the background.

removing calculated 35  $PM_{2.5}$  concentrations from the fixed-emission simulation one by one and by generating probabilistic distributions based on the 34 remaining data sets. The mean and standard deviation of the 35 repeated calculations are  $3 \times 10^{-17} \pm 5 \times 10^{-17}$  and  $0.04 \pm 0.001$ , respectively, indicating a very high degree of robustness.

In fact, the probabilistic functions can be derived either on an annual basis or on any temporal scale from a daily to seasonal basis. Figure 3 shows typical examples of the probabilistic functions for a typical grid cell (Guangzhou, China) on annual (a), monthly (b), and daily (c) scales. The majority of these functions reflect typical normal distributions, which is more evident on a shorter time scale. On an annual scale, the annual mean  $PM_{2.5}$  concentration changes considerably with a coefficient of variation (CV) of 14%. Even without any change in emissions, the annual mean  $PM_{2.5}$  concentration presents a 48% chance of increasing or may decrease by more than 10%. This means that while emission-mitigation measures can reduce ambient  $PM_{2.5}$  concentrations by 10% in a single year for this grid cell, there is a more than 20% chance of the observed annual mean concentration not declining at all or even of increasing. Similarly, the likelihood of the annual mean decreasing by more than 20% is also higher than 20%. Therefore, simply comparing annual mean  $PM_{2.5}$  concentrations of two consecutive years without taking meteorological conditions into consideration can be misleading. Upon reducing the time scale from annual to monthly and daily, the variation in probabilistic functions increases. CV values for monthly and daily  $PM_{2.5}$  concentrations increase to 29% and 38%, respectively, for the selected grid cell, which are significantly higher values than those found for annual data and which can be explained by the fact that daily and monthly meteorological conditions vary more dramatically than emissions. Therefore, monthly meteorological factor-forced changes are more random than those observed on an annual scale. With constant emissions there is a more than 50% probability of a 20% change occurring in monthly mean  $PM_{2.5}$  concentrations. Therefore, it is even riskier to directly compare mean  $PM_{2.5}$  concentrations of a given month to those for the same period of a previous year while disregarding random confounding meteorological effects.

The random variation observed in the calculated probabilistic function is a direct indicator of the extent of confounding meteorological effects on individual grid cells. To quantify overall variations on a global scale, annual mean-based CVs were calculated for all grid cells. Corresponding results are shown in Figure S12 as a cumulative distribution of CVs for all grid cells. The mean and standard deviation of the CV values are  $16 \pm 11\%$  (median is 14.2%) with a maximum value of 109%. On average, confounding meteorological factors

can lead to more than one-sixth of a variation at 28% for all model grid cells. The contribution can be as high as 100% in extreme cases. As discussed above, short-term variations observed over less than one year are even larger. When monthly data are used, the mean and standard deviation of the CV values are  $65 \pm 35\%$ , showing stronger seasonal variations. The maximum CV of an individual grid cell can reach 200% on a monthly scale. Again, significant autocorrelations (Moran's index = 0.59,  $p < 0.05$ ) were found for the probabilistic functions (CVs) on an annual scale, denoting continuity in meteorological effects across space.

The annual change in confounding meteorological effects on globally averaged  $PM_{2.5}$  concentrations, defined as a normalized global average  $PM_{2.5}$  anomaly for individual year from the 35 year mean, was calculated from 1980 to 2014 based on the fixed-emission simulation. The deviations observed reflect the average influence of annual meteorological conditions on annual mean  $PM_{2.5}$  concentrations on a global scale. It should be noted that the annual deviation observed in 2014 was the smallest, showing that using meteorological parameters for 2014 as a "normal" year for our fixed-meteorological simulations is the best choice for the 35 years studied. Such annual changes are often affected by global atmospheric circulation.<sup>50</sup> It is interesting to observe that the interannual anomalies of meteorological effects are significantly correlated with Arctic oscillation (AO), which is shown as solid dots in Figure 4 ( $r = 0.66$ ,  $p < 0.05$ ). Some regional studies also show a similar relationship. For example, it was reported that enhanced dust emissions observed across Saharan regions and the increasing frequency of haze episodes recorded in northern China are associated with the positive phase of AO.<sup>10,51</sup>

To further illustrate spatial variations in meteorological-induced variation,  $UI_{95}$  values are mapped in Figure S13 in

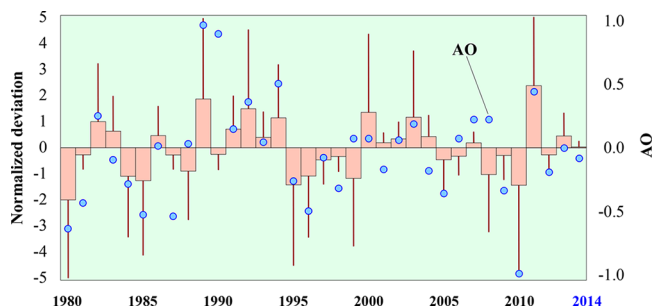


**Figure 4.** Normalized global average deviation of  $PM_{2.5}$  concentrations from the mean value for the 35 years spanning from 1980 to 2014 (bars). The results are based on a fixed-emission simulation conducted at the global scale. Standard deviations are shown as dark red lines. The blue dots denote Arctic oscillation.

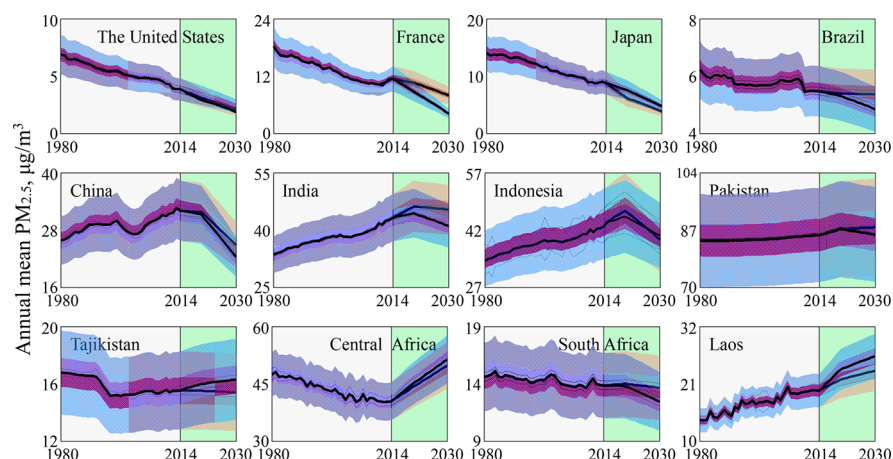


**Figure 5.** Temporal trends of  $\text{PM}_{2.5}$  concentrations for 12 countries for 1980 to 2030 based on the RCP2.6 (blue) and RCP8.5 (orange) emission scenarios. Emission-driven trends are shown as medians (black lines) with a 90% confidence interval (black dash lines). Potential fluctuations induced by meteorological confounding effects are shown as shaded areas as  $\text{UI}_{50}$  (dark shaded area) and  $\text{UI}_{95}$  (light shaded area).

both absolute and relative terms. The global average  $\text{UI}_{95}$  of annual  $\text{PM}_{2.5}$  concentrations was measured as  $4.9 \mu\text{g}/\text{m}^3$  (40%). Hot regions of absolute variation exhibit strong meteorological variations. In addition to areas around deserts (e.g., the southern Sahara and the Middle East) where dust forms a major component of  $\text{PM}_{2.5}$  emissions and where concentrations are subject to synoptic-scale weather patterns,<sup>51</sup> strong variations in  $\text{PM}_{2.5}$  concentrations can be observed in heavily polluted regions such as the North China Plain (NCP) and likely are due to interactions between high emissions and highly variable meteorological patterns.<sup>9,46</sup> On the other hand, relatively large values of relative terms are often observed in regions with low levels of population density and low  $\text{PM}_{2.5}$  concentrations. For example, very high levels of relative variability were found in high-latitude regions and coastal areas, where background  $\text{PM}_{2.5}$  concentrations are very low. In most high-emission regions (e.g., eastern China, India, Europe, the United States), although  $\text{PM}_{2.5}$  variations induced by meteorological conditions are lower, high  $\text{PM}_{2.5}$  levels can increase absolute variations on a considerable scale. For example, the  $\text{UI}_{95}$  for northern India and for the NCP are as high as 11.5 and  $20.6 \mu\text{g}/\text{m}^3$ , respectively.

**Model Application.** When the regression model predictions and probabilistic functions are combined, annual mean  $\text{PM}_{2.5}$  concentration trends driven by emissions coupled with meteorological effects can be quantified. The concentration predicted by the regression model provides an estimation of the annual mean  $\text{PM}_{2.5}$  under given emissions and average meteorological conditions, whereas a range derived from the probabilistic function at a fixed probability (e.g., 95%) shows fluctuation associated with random variations of meteorological parameters. This approach was then applied to simulate global historical temporal trends of  $\text{PM}_{2.5}$  concentrations from 1980 to 2014 and to project future trends from 2015 to 2030. Emission-driven trends of global annual mean  $\text{PM}_{2.5}$  concentrations prior to 2015 were calculated from the grid cell regression models based on PKU series emission inventories<sup>19</sup> and from the Representative Concentration Pathways (RCP)2.6 and RCP8.5 emission scenario models run for after 2014<sup>52,53</sup> using emissions for 2014 as a baseline. The results are denoted by the solid line in Figure S14a. In the figure, meteorological condition-induced variation ranges are shown by the darkly shaded  $\text{UI}_{50}$  and

lightly shaded  $\text{UI}_{95}$ . We further assume that meteorological conditions for 2014 used as a “normal” year can be extended to future years. For the past 35 years, global annual mean  $\text{PM}_{2.5}$  concentrations decreased slightly from  $13.1 \mu\text{g}/\text{m}^3$  ( $10.4\text{--}16.1 \mu\text{g}/\text{m}^3$  as  $\text{UI}_{50}$ ) to  $12.1 \mu\text{g}/\text{m}^3$  ( $9.8\text{--}14.6 \mu\text{g}/\text{m}^3$ ), and decreasing trends tend to continue in the future at a slightly faster rate, which could be attributed to increasing awareness and to emission-mitigation efforts made by many developing countries, especially China. We found slight differences in projected  $\text{PM}_{2.5}$  levels between the two emission scenarios on a global scale prior to 2030. It should be noted that the probability functions were developed based on gridded meteorological parameters. When the results are presented on an area with more than one grid cell, such as a country, a city, or even the globe, the calculated UI values are simply averaged over grid cells covering the area. This practice is based on the assumption that all meteorological confounding factors do not vary significantly within the region of concern. This applies to a relatively small region such as the NCP, where a somewhat uniform surface pressure with small pressure gradients is often observed, which in turn produces fewer altered wind and temperature fields across the NCP. However, for a larger region such as China or a region with complex terrain, this assumption would lead to an over-estimation of UI values. Unfortunately, the accuracy of the UI estimation is difficult to enhance, as spatial similarities in changes of meteorological parameters are difficult to quantify. To further validate the model-calculated  $\text{PM}_{2.5}$  concentrations using the regression models, the calculated  $\text{PM}_{2.5}$  concentrations for before 2014 are compared to those observed from various monitoring stations (grid cells) over various years in Figure S14b,c. Both calculated annual mean concentrations (dots) and UI values (bars: panel b,  $\text{UI}_{50}$ ; panel c,  $\text{UI}_{95}$ ) are shown, indicating a good agreement.

The method was further applied to various countries to predict annual mean  $\text{PM}_{2.5}$  concentrations subject to the changes in emissions. Corresponding results are shown in Figure 5 for 12 countries. The projected  $\text{PM}_{2.5}$  trend for 1980 to 2030 from the regression model was obtained based on RCP2.6 and RCP8.5 emission scenarios.<sup>52,53</sup> In general, these trends and UI values vary significantly across countries. Relatively high levels of variability observed for some countries are associated with stronger changes in meteorological

conditions and especially for monsoon regions (e.g., China and Pakistan) where the strength of prevailing monsoons play an important role in aerosol production and dispersion.<sup>10,54</sup> The results also show that for developed countries such as the United States, France, and Japan, past declines in  $PM_{2.5}$  will remain with slight differences between RCP2.6 and RCP8.5 predictions. Trends for France are an exception, as the RCP2.6 assumes a much stronger decrease in pollutant emissions and hence in  $PM_{2.5}$  concentrations. Predicted  $PM_{2.5}$  concentration trends vary substantially across developing countries. In China, annual mean  $PM_{2.5}$  concentrations tend to decrease continuously, which is consistent with considerable efforts made to curb air pollution in recent years.<sup>16</sup> For other developing countries such as India and Indonesia,  $PM_{2.5}$  concentrations are projected to increase continuously until 2020 if the proposed emission scenarios are not altered. As the RCPs data set provides emission data at a decadal temporal resolution, tipping points from emission incline to decline cannot be precisely identified. Nevertheless, these trends imply that although severe levels of air pollution have spurred widespread awareness and concern from governments and the public, efficient mitigation is still lacking in most developing countries. Meanwhile, it is very likely that air  $PM_{2.5}$  concentrations will increase continuously in coming years in developing countries such as Laos and in Central Africa.

Figure S15 shows three examples of predicted historical and future trends of  $PM_{2.5}$  concentrations for three cities for which recent monitoring data are available, based on the RCP2.6 and RCP8.5 emission scenarios<sup>52,53</sup> for 1980 to 2030. For the city of New York,  $PM_{2.5}$  monitoring data for after 2014 suggest that emission-reduction rates likely range between the two scenarios, which are not remarkably different in the first place. For New Delhi, although the observed values still fall within the  $UI_{95}$  range, concentrations reported for the last three years exceed the predicted means. Although unusual meteorological conditions could play a critical role in increasing concentrations, relatively high levels of  $PM_{2.5}$  observed for 2014 and 2016 may indicate accelerated increases in emission and pollution levels. Numerous studies have reported high levels of air pollution in India in recent years.<sup>55</sup> Beijing is one of the most heavily contaminated cities in northern China. On the basis of both RCP2.6 and RCP8.5 emission scenarios, we find a slight decline in  $PM_{2.5}$  concentrations after 2014. However, the measured annual mean  $PM_{2.5}$  concentrations from 2014 to 2016 are well below the predicted ones and even fall below the lower bound of the 95% uncertainty interval. It is likely that mitigation measures applied in the city were more effective than what was planned in RCP scenarios.

In summary, the novel method developed in this study serves as a useful tool for quantifying emission-induced changes in  $PM_{2.5}$  concentrations by excluding confounding meteorological effects. The approach involves less computation than an atmospheric chemical transport model; hence, it can be used in quantitative environments, for health assessments of  $PM_{2.5}$ , and to evaluate the effectiveness of mitigation efforts. Importantly, we learned from this study that long-term trends rather than declines occurring over a single year are critical to consider when evaluating the effectiveness of mitigation measures while considering meteorology-induced  $PM_{2.5}$  fluctuations.

## ■ ASSOCIATED CONTENT

### § Supporting Information

The Supporting Information is available free of charge on the ACS Publications website at DOI: 10.1021/acs.est.8b02685.

Detailed results of the sensitivity analysis for key pollutants, various model validations, spatial distributions of major meteorological parameters, comparisons drawn between emissions and  $PM_{2.5}$  concentrations, frequency distributions of emissions and  $PM_{2.5}$  concentrations, spatial distributions of regression model  $R^2$  values, meteorological effect-induced variations, cumulative distributions of CVs, and predicted trends for three cities (PDF)

## ■ AUTHOR INFORMATION

### Corresponding Author

\*Phone and fax: +86-10-62751938; e-mail: taos@pku.edu.cn.

### ORCID

Jianmin Ma: 0000-0002-6593-570X

Guofeng Shen: 0000-0002-7731-5399

Huizhong Shen: 0000-0003-1335-8477

Junfeng Liu: 0000-0002-7199-6357

Eddy Y. Zeng: 0000-0002-0859-7572

Shu Tao: 0000-0002-7374-7063

### Notes

The authors declare no competing financial interest.

## ■ ACKNOWLEDGMENTS

This work was funded by the National Natural Science Foundation of China (Grant 41571130010, 41390240, and 41629101), the 111 program (B14001), and the Undergraduate Student Research Training Program.

## ■ REFERENCES

- (1) Lelieveld, J.; Evans, J. S.; Fnais, M.; Giannadaki, D.; Pozzer, A. The contribution of outdoor air pollution sources to premature mortality on a global scale. *Nature* **2015**, *525* (7569), 367–371.
- (2) Cohen, A. J.; Brauer, M.; Burnett, R.; Anderson, H. R.; Frostad, J.; Estep, K.; Balakrishnan, K.; Brunekreef, B.; Dandona, L.; Dandona, R.; Feigin, V.; Freedman, G.; Hubbell, B.; Jobling, A.; Kan, H.; Knibbs, L.; Liu, Y.; Martin, R.; Morawska, L.; Pope, C. A., III; Shin, H.; Straif, K.; Shaddick, G.; Thomas, M.; van Dingenen, R.; van Donkelaar, A.; Vos, T.; Murray, C. J. L.; Forouzanfar, M. H. Estimates and 25-year trends of the global burden of disease attributable to ambient air pollution: an analysis of data from the Global Burden of Diseases Study 2015. *Lancet* **2017**, *389* (10082), 1907–1918.
- (3) Ansari, A. S.; Pandis, S. N. Response of Inorganic PM to Precursor Concentrations. *Environ. Sci. Technol.* **1998**, *32*, 2706–2714.
- (4) Hueglin, C.; Gehrig, R.; Baltensperger, U.; Gysel, M.; Monn, C.; Vonmont, H. Chemical characterisation of  $PM_{2.5}$ ,  $PM_{10}$  and coarse particles at urban, near-city and rural sites in Switzerland. *Atmos. Environ.* **2005**, *39* (4), 637–651.
- (5) Liu, J.; Mauzerall, D. L.; Chen, Q.; Zhang, Q.; Song, Y.; Peng, W.; Klimont, Z.; Qiu, X.; Zhang, S.; Hu, M.; Lin, W.; Smith, K. R.; Zhu, T. Air pollutant emissions from Chinese households: A major and underappreciated ambient pollution source. *Proc. Natl. Acad. Sci. U. S. A.* **2016**, *113* (28), 7756–7761.
- (6) Zhang, H.; Hu, D.; Chen, J.; Ye, X.; Wang, S. X.; Hao, J. M.; Wang, L.; Zhang, R.; An, Z. Particle size distribution and polycyclic aromatic hydrocarbons emissions from agricultural crop residue burning. *Environ. Sci. Technol.* **2011**, *45* (13), 5477–5482.

- (7) Tai, A. P. K.; Mickley, L. J.; Jacob, D. J. Correlations between fine particulate matter (PM<sub>2.5</sub>) and meteorological variables in the United States: Implications for the sensitivity of PM<sub>2.5</sub> to climate change. *Atmos. Environ.* **2010**, *44* (32), 3976–3984.
- (8) DeGaetano, A. Temporal, spatial and meteorological variations in hourly PM<sub>2.5</sub> concentration extremes in New York City. *Atmos. Environ.* **2004**, *38* (11), 1547–1558.
- (9) Sun, Y.; Chen, C.; Zhang, Y.; Xu, W.; Zhou, L.; Cheng, X.; Zheng, H.; Ji, D.; Li, J.; Tang, X.; Fu, P.; Wang, Z. Rapid formation and evolution of an extreme haze episode in Northern China during winter 2015. *Sci. Rep.* **2016**, *6*, 27151.
- (10) Zou, Y.; Wang, Y.; Zhang, Y.; Koo, J. H. Arctic sea ice, Eurasia snow, and extreme winter haze in China. *Sci. Adv.* **2017**, *3* (3), e1602751.
- (11) Guo, S.; Hu, M.; Zamora, M. L.; Peng, J.; Shang, D.; Zheng, J.; Du, Z.; Wu, Z.; Shao, M.; Zeng, L.; Molina, M. J.; Zhang, R. Elucidating severe urban haze formation in China. *Proc. Natl. Acad. Sci. U. S. A.* **2014**, *111* (49), 17373–17378.
- (12) Wang, Y.; Yao, L.; Wang, L.; Liu, Z.; Ji, D.; Tang, G.; Zhang, J.; Sun, Y.; Hu, B.; Xin, J. Mechanism for the formation of the January 2013 heavy haze pollution episode over central and eastern China. *Sci. China: Earth Sci.* **2014**, *57* (1), 14–25.
- (13) Zhao, X. J.; Zhao, P. S.; Xu, J.; Meng, W.; Pu, W. W.; Dong, F.; He, D.; Shi, Q. F. Analysis of a winter regional haze event and its formation mechanism in the North China Plain. *Atmos. Chem. Phys.* **2013**, *13* (11), 5685–5696.
- (14) Shen, L.; Mickley, L. J.; Murray, L. T. Influence of 2000–2050 climate change on particulate matter in the United States: results from a new statistical model. *Atmos. Chem. Phys.* **2017**, *17*, 4355–4367.
- (15) Ministry of Environmental Protection of the People's Republic of China (MEP). [http://www.zhb.gov.cn/gkml/hbb/qt/201707/t20170725\\_418538.htm](http://www.zhb.gov.cn/gkml/hbb/qt/201707/t20170725_418538.htm) (accessed December 2017).
- (16) Qin, Y.; Wagner, F.; Scovronick, N.; Peng, W.; Yang, J.; Zhu, T.; Smith, K. R.; Mauzerall, D. L. Air quality, health, and climate implications of China's synthetic natural gas development. *Proc. Natl. Acad. Sci. U. S. A.* **2017**, *114* (19), 4887–4892.
- (17) Liu, Y.; Wu, Z.; Wang, Y.; Xiao, Y.; Gu, F.; Zheng, J.; Tan, T.; Shang, D.; Wu, Y.; Zeng, L.; Hu, M.; Bateman, A. P.; Martin, S. T. Submicrometer Particles Are in the Liquid State during Heavy Haze Episodes in the Urban Atmosphere of Beijing, China. *Environ. Sci. Technol. Lett.* **2017**, *4* (10), 427–432.
- (18) Emmons, L. K.; Walters, S.; Hess, P. G.; Lamarque, J. F.; Pfister, G. G.; Fillmore, D.; Granier, C.; Guenther, A.; Kinnison, D.; Laepple, T.; Orlando, J.; Tie, X.; Tyndall, G.; Wiedinmyer, C.; Baughcum, S. L.; Kloster, S. Description and evaluation of the Model for Ozone and Related chemical Tracers, version 4 (MOZART-4). *Geosci. Model Dev.* **2010**, *3*, 43–67.
- (19) Peking University Inventory Dataset, version 2. <http://inventory.pku.edu.cn/> (accessed July 2017).
- (20) Crippa, M.; Guizzardi, D.; Muntean, M.; Schaaf, E.; Dentener, F.; van Aardenne, J. A.; Monni, S.; Doering, U.; Olivier, J. G. J.; Pagliari, V.; Janssens-Maenhout, G. Gridded Emissions of Air Pollutants for the period 1970–2012 within EDGAR v4.3.2. *Earth Syst. Sci. Data Discuss.* **2018**, DOI: 10.5194/essd-2018-31.
- (21) Janssens-Maenhout, G.; Crippa, M.; Guizzardi, D.; Dentener, F.; Muntean, M.; Pouliot, G.; Keating, T.; Zhang, Q.; Kurokawa, J.; Wankmüller, R.; Denier van der Gon, H.; Kuenen, J. J. P.; Klimont, Z.; Frost, G.; Darras, S.; Koffi, B.; Li, M. HTAP\_v2.2: a mosaic of regional and global emission grid maps for 2008 and 2010 to study hemispheric transport of air pollution. *Atmos. Chem. Phys.* **2015**, *15*, 11411–11432.
- (22) Sindelarova, K.; Granier, C.; Bouarar, I.; Guenther, A.; Tilmes, S.; Stavrakou, T.; Müller, J. F.; Kuhn, U.; Stefani, P.; Knorr, W. Global data set of biogenic VOC emissions calculated by the MEGAN model over the last 30 years. *Atmos. Chem. Phys.* **2014**, *14* (17), 9317–9341.
- (23) van der Werf, G. R.; Randerson, J. T.; Giglio, L.; van Leeuwen, T. T.; Chen, Y.; Rogers, B. M.; Mu, M.; van Marle, M. J. E.; Morton, D. C.; Collatz, G. J.; Yokelson, R. J.; Kasibhatla, P. S. Global fire emissions estimates during 1997–2016. *Earth Syst. Sci. Data* **2017**, *9* (2), 697–720.
- (24) Kalnay, E.; Kanamitsu, M.; Kistler, R.; Collins, W.; Deaven, D.; Gandin, L.; Iredell, M.; Saha, S.; White, G.; Woollen, J.; Zhu, Y.; Chelliah, M.; Ebisuzaki, W.; Higgins, W.; Janowiak, J.; Mo, K. C.; Ropelewski, C.; Wang, J.; Leetmaa, A.; Reynolds, R.; Jenne, R.; Joseph, D. The NCEP/NCAR 40-Year Reanalysis Project. *Bull. Am. Meteorol. Soc.* **1996**, *77*, 437–471.
- (25) Levy, R. C.; Remer, L. A.; Kleidman, R. G.; Mattoo, S.; Ichoku, C.; Kahn, R.; Eck, T. F. Global evaluation of the Collection 5 MODIS dark-target aerosol products over land. *Atmos. Chem. Phys.* **2010**, *10* (21), 10399–10420.
- (26) van Donkelaar, A.; Martin, R. V.; Brauer, M.; Kahn, R.; Levy, R.; Verduzco, C.; Villeneuve, P. J. Global estimates of ambient fine particulate matter concentrations from satellite-based aerosol optical depth: development and application. *Environ. Health Perspect.* **2010**, *118* (6), 847–855.
- (27) IBM SPSS Statistics Manuals. <https://www-01.ibm.com/support/docview.wss?uid=swg27038407#en> (accessed 2015).
- (28) MathWorks Documentation for MATLAB. <https://www.mathworks.com/help/matlab/index.html> (accessed December 2016).
- (29) Mahmud, A.; Barsanti, K. Improving the representation of secondary organic aerosol (SOA) in the MOZART-4 global chemical transport model. *Geosci. Model Dev.* **2013**, *6*, 961–980.
- (30) Valorso, R.; Aumont, B.; Camredon, M.; Raventos-Duran, T.; Mouchel-Vallon, C.; Ng, N. L.; Seinfeld, J. H.; Lee-Taylor, J.; Madronich, S. Explicit modelling of SOA formation from  $\alpha$ -pinene photooxidation: sensitivity to vapour pressure estimation. *Atmos. Chem. Phys.* **2011**, *11*, 6895–6910.
- (31) Zhang, L.; Liu, L.; Zhao, Y.; Gong, S.; Zhang, X.; Henze, D. K.; Capps, S. L.; Fu, T. M.; Zhang, Q.; Wang, Y. Source attribution of particulate matter pollution over North China with the adjoint method. *Environ. Res. Lett.* **2015**, *10* (8), 084011.
- (32) Heo, J.; Adams, P. J.; Gao, H. O. Public Health Costs of Primary PM<sub>2.5</sub> and Inorganic PM<sub>2.5</sub> Precursor Emissions in the United States. *Environ. Sci. Technol.* **2016**, *50* (11), 6061–6070.
- (33) Wang, R.; Tao, S.; Shen, H.; Huang, Y.; Chen, H.; Balkanski, Y.; Boucher, O.; Ciais, P.; Shen, G.; Li, W.; Zhang, Y.; Chen, Y.; Lin, N.; Su, S.; Li, B.; Liu, J.; Liu, W. Trend in global black carbon emissions from 1960 to 2007. *Environ. Sci. Technol.* **2014**, *48* (12), 6780–6787.
- (34) Huang, Y.; Shen, H.; Chen, H.; Wang, R.; Zhang, Y.; Su, S.; Chen, Y.; Lin, N.; Zhuo, S.; Zhong, Q.; Wang, X.; Liu, J.; Li, B.; Liu, W.; Tao, S. Quantification of global primary emissions of PM<sub>2.5</sub>, PM<sub>10</sub>, and TSP from combustion and industrial process sources. *Environ. Sci. Technol.* **2014**, *48* (23), 13834–13843.
- (35) Bell, M. L.; Dominici, F.; Ebisu, K.; Zeger, S. L.; Samet, J. M. Spatial and temporal variation in PM(2.5) chemical composition in the United States for health effects studies. *Environ. Health Perspect.* **2007**, *115* (7), 989–995.
- (36) Pérez, N.; Pey, J.; Querol, X.; Alastuey, A.; López, J. M.; Viana, M. Partitioning of major and trace components in PM<sub>10</sub>-PM<sub>2.5</sub>-PM<sub>1</sub> at an urban site in Southern Europe. *Atmos. Environ.* **2008**, *42*, 1677–1691.
- (37) Dawson, J. P.; Adams, P. J.; Pandis, S. N. Sensitivity of PM<sub>2.5</sub> to climate in the Eastern US: a modeling case study. *Atmos. Chem. Phys.* **2007**, *7*, 4295–4309.
- (38) Jiménez-Guerrero, P.; Gomez-Navarro, J. J.; Jerez, S.; Lorente-Plazas, R.; Garcia-Valero, J. A.; Montavez, J. P. Isolating the effects of climate change in the variation of secondary inorganic aerosols (SIA) in Europe for the 21st century (1991–2100). *Atmos. Environ.* **2011**, *45* (4), 1059–1063.
- (39) Du, C.; Liu, S.; Yu, X.; Li, X.; Chen, C.; Peng, Y.; Dong, Y.; Dong, Z.; Wang, F. Urban boundary layer height characteristics and relationship with particulate matter mass concentrations in Xi'an, central China. *Aerosol Air Qual. Res.* **2013**, *13* (5), 1598–1607.
- (40) Tiwari, S.; Srivastava, A. K.; Bisht, D. S.; Parmita, P.; Srivastava, M. K.; Attri, S. D. Diurnal and seasonal variations of black carbon and

PM<sub>2.5</sub> over New Delhi, India: Influence of meteorology. *Atmos. Res.* **2013**, *125–126*, 50–62.

(41) Shahsavani, A.; Naddafi, K.; Haghhighifard, N. J.; Mesdaghinia, A.; Yunesian, M.; Nabizadeh, R.; Arahami, M.; Sowlat, M. H.; Yarahmadi, M.; Saki, H.; Alimohamadi, M.; Nazmara, S.; Motevalian, S. A.; Goudarzi, G. The evaluation of PM<sub>10</sub>, PM<sub>2.5</sub>, and PM<sub>1</sub> concentrations during the Middle Eastern Dust (MED) events in Ahvaz, Iran, from april through september 2010. *J. Arid Environ.* **2012**, *77*, 72–83.

(42) Chen, H.; Huang, Y.; Shen, H.; Chen, Y.; Ru, M.; Chen, Y.; Lin, N.; Su, S.; Zhuo, S.; Zhong, Q.; Wang, X.; Liu, J.; Li, B.; Tao, S. Modeling temporal variations in global residential energy consumption and pollutant emissions. *Appl. Energy* **2016**, *184*, 820–829.

(43) Suri, V.; Chapman, D. Economic growth, trade and energy: implications for the environmental Kuznets curve. *Ecol. Econ.* **1998**, *25*, 195–208.

(44) Zheng, M.; Salmon, L. G.; Schauer, J. J.; Zeng, L.; Kiang, C. S.; Zhang, Y.; Cass, G. R. Seasonal trends in PM<sub>2.5</sub> source contributions in Beijing, China. *Atmos. Environ.* **2005**, *39* (22), 3967–3976.

(45) Gao, J.; Woodward, A.; Vardoulakis, S.; Kovats, S.; Wilkinson, P.; Li, L.; Xu, L.; Li, J.; Yang, J.; Cao, L.; Liu, X.; Wu, H.; Liu, Q. Haze, public health and mitigation measures in China: A review of the current evidence for further policy response. *Sci. Total Environ.* **2017**, *578*, 148–157.

(46) Zheng, G. J.; Duan, F. K.; Su, H.; Ma, Y. L.; Cheng, Y.; Zheng, B.; Zhang, Q.; Huang, T.; Kimoto, T.; Chang, D.; Pöschl, U.; Cheng, Y. F.; He, K. B. Exploring the severe winter haze in Beijing: the impact of synoptic weather, regional transport and heterogeneous reactions. *Atmos. Chem. Phys.* **2015**, *15* (6), 2969–2983.

(47) Cai, W.; Li, K.; Liao, H.; Wang, H.; Wu, L. Weather conditions conducive to Beijing severe haze more frequent under climate change. *Nat. Clim. Change* **2017**, *7* (4), 257–262.

(48) Kelly, J.; Makar, P. A.; Plummer, D. A. Projections of mid-century summer air-quality for North America: effects of changes in climate and precursor emissions. *Atmos. Chem. Phys.* **2012**, *12* (12), 5367–5390.

(49) Tie, X.; Zhang, Q.; He, H.; Cao, J.; Han, S.; Gao, Y.; Li, X.; Jia, X. C. A budget analysis of the formation of haze in Beijing. *Atmos. Environ.* **2015**, *100*, 25–36.

(50) Hedegaard, G. B.; Christensen, J. H.; Brandt, J. The relative importance of impacts from climate change vs. emissions change on air pollution levels in the 21st century. *Atmos. Chem. Phys.* **2013**, *13* (7), 3569–3585.

(51) Pey, J.; Querol, X.; Alastuey, A.; Forastiere, F.; Stafoggia, M. African dust outbreaks over the Mediterranean Basin during 2001–2011: PM<sub>10</sub> concentrations, phenomenology and trends, and its relation with synoptic and mesoscale meteorology. *Atmos. Chem. Phys.* **2013**, *13* (3), 1395–1410.

(52) Riahi, K.; Grübler, A.; Nakicenovic, N. Scenarios of long-term socio-economic and environmental development under climate stabilization. *Technol. Forecast. Soc.* **2007**, *74* (7), 887–935.

(53) van Vuuren, D. P.; den Elzen, M. G. J.; Lucas, P. L.; Eickhout, B.; Strengers, B. J.; van Ruijven, B.; Wonink, S.; van Houdt, R. Stabilizing greenhouse gas concentrations at low levels: an assessment of reduction strategies and costs. *Clim. Change* **2007**, *81* (2), 119–159.

(54) Mansha, M.; Ghauri, B.; Rahman, S.; Amman, A. Characterization and source apportionment of ambient air particulate matter (PM<sub>2.5</sub>) in Karachi. *Sci. Total Environ.* **2012**, *425*, 176–183.

(55) Li, C.; McLinden, C.; Fioletov, V.; Krotkov, N.; Carn, S.; Joiner, J.; Streets, D.; He, H.; Ren, X.; Li, Z.; Dickerson, R. R. India Is Overtaking China as the World's Largest Emitter of Anthropogenic Sulfur Dioxide. *Sci. Rep.* **2017**, *7*, 14304.